Hot, dense, millimeter-scale, high-*Z* plasmas for laser-plasma interactions studies

B. H. Failor,[1,*] J. C. Fernandez,[1] B. H. Wilde,[1] A. L. Osterheld,[2] J. A. Cobble,[1] and P. L. Gobby[1]
[1]*Los Alamos National Laboratory, P.O. Box 1660, Los Alamos, New Mexico 87545*
[2]*Lawrence Livermore National Laboratory, P.O. Box 808, Livermore, California 94551*
(Received 17 August 1998; revised manuscript received 4 January 1999)

We have designed and produced hot, millimeter-scale, high-*Z* plasmas of interest for National Ignition Facility hohlraum target design. Using a high-*Z* gas fill produces electron temperatures in the 3.5–6-keV range, the highest temperatures measured to date for high-density ($10^{21}\,e/\mathrm{cm}^3$) laser-heated plasmas, and much higher than the 3 keV found for low-*Z* (neopentane) fills. These measurements are in good agreement with the target design calculations, and the *L*-shell spectroscopic approach used to estimate the electron temperature has certain advantages over traditional *K*-shell approaches. [S1063-651X(99)15205-X]

PACS number(s): 52.50.Jm, 52.25.Nr, 52.35.Nx, 52.70.La

INTRODUCTION

The National Ignition Facility (NIF) will implode fuel capsules in laser-heated hohlraums to investigate the physics of fusion ignition and burn in the laboratory. Plasma produced in these hohlraums can potentially reflect away a large fraction of the incident laser energy via laser plasma instabilities (LPI's), such as stimulated Brillouin scattering (SBS) and stimulated Raman scattering (SRS). NIF-scale plasmas have been produced in the laboratory in order to estimate the expected scattered light levels [1]. Both the low-*Z* gas fill and the high-*Z* material ablated from the hohlraum wall produce plasmas susceptible to, or that can support, LPI. *K*-shell x-ray emission from dopants, such as Ti/Cr [2–4] and Ar/Cl [5], have provided estimates of electron temperature T_e in low-*Z* gas fills. In this paper we describe target designs developed to investigate SRS and SBS in high-*Z* gas-fill plasmas, and how we have used *L*-shell x-ray emissions to estimate the T_e in these plasmas. The measured electron temperatures for these high-*Z* fills, 3.5–6 keV, are much higher than for low-*Z* fills (3 keV for neopentane) and are actually the highest temperatures measured to date for high-density ($10^{21}\,e/\mathrm{cm}^3$) laser-heated plasmas. For this reason the plasmas are of interest for efficient generation of x rays in the 4–7 keV energy range [6]. These T_e estimates are compared with results from a numerical design tool, LASNEX [7], which is used to predict NIF hohlraum performance. T_e is an important parameter in these high-*Z* plasmas because it can determine the types of instabilities that are most active [8]. Although the *L*-shell x-ray emission is more difficult to calculate, it has some advantages over *K*-shell emission as a temperature diagnostic, including faster time response, better signal-to-noise ratio, and flatter instrument sensitivity.

APPROACH

In this section we describe the experimental conditions, the diagnostic measurements, and the numerically predicted scaling of line ratios. The experimental conditions can be considered the ''system inputs,'' and the diagnostic measurements the ''system outputs.''

The system inputs include the target and the laser. For this set of experiments, toroidal hohlraum targets were shot. The hohlraum has a 25-μm-thick gold wall, and is 3.6 mm in diameter and 1.6 mm in length. The hohlraum corners are not sharp, but rather have a 0.7-mm radius of curvature [9]. Often a 185-μm diagnostic slot was present at the hohlraum midplane, sealed with 0.6- or 1.0-μm-thick Mylar, which allowed the spectrograph (described below) to look into the center of the hohlraum. The primary fill gas was xenon (Xe), with deuterium (D_2) or neopentane (C_5H_{12}) sometimes added. The gas fill was sealed inside the hohlraum with silicon nitride windows glued on each end.

The laser energy entered the hohlraum through the two silicon nitride windows [9]. The ten Nova beams, five incident from the east and five from the west, were operated in the blue at 351 nm. To obtain the desired plasma conditions, a 1.4-nsec-long laser pulse, rising about 50% in power with time, was used. Nine beams turned on simultaneously to ionize and heat the target plasma. A tenth beam, which acted as the SBS/SRS probe, turned on later, when the desired hot, long-scale-length plasma was formed.

The plasma conditions that LASNEX predicts at 0.9 nsec from the beginning of the heating pulse for a 67% Xe and 33% D_2 fill are shown in Fig. 1. The different parameters are plotted versus the distance along the laser beam path, from the window to the wall. The weak density and temperature gradients are expected to be conducive to LPI growth.

The Xe emission lines (the ''system outputs,'' in this case) were measured using spatially and time-resolving crystal spectrographs [2]. Multichannel-plate (MCP) based gated x-ray imagers (GXI's) with four strip lines, each recorded four independently timed spectra on each shot. An array of horizontal slits spatially resolved the spectra in the vertical direction, and a flat TlAP crystal provided spectral dispersion. As indicated in Fig. 2, measurements were made along three different lines of sight: laser entrance hole (LEH), laser beam path, and midplane. As discussed below, the plasma conditions and the volume of plasma viewed along these lines of sight were different.

A numerical model [10] predicts how the Xe emission depends on plasma conditions. Xe 3-2 transitions have been

*Permanent address: Maxwell Physics International, 2700 Merced Street, San Leandro, CA 94577.

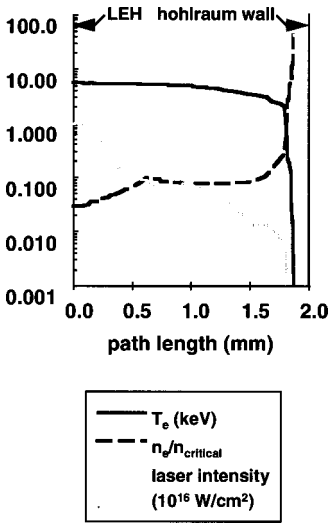

FIG. 1. LASNEX predictions for electron temperature (T_e) and electron density (n_e) along the laser beam path from laser entrance hole (LEH) to hohlraum wall at 0.9 nsec after start of laser pulse. The hohlraum was filled with a 67/33 mixture of Xe/D_2, and the laser was fired at full power (30 kJ). T_e in the LEH is 5.4 keV.

used to estimate core conditions in inertial confinement fusion implosions [10], but we have focused on Xe 4-2 lines that have been used in the past to diagnose magnetic fusion plasmas [11], namely, the Ne-like $2p_{3/2}$-$4d_{5/2}$ resonant line and the Na like $3l4l'$ satellite. The same 4-2 transitions for Y have been measured in another laser-produced plasma [12]. Mg-like satellite emission is also present, but predicting its level is much more complex computationally because so many additional atomic levels are needed for the calculation. A plot of how the Na-like to Ne-like ratio varies with electron temperature at two different electron densities, 10^{20} and 10^{21} e/cm^3, is shown in Fig. 3. Given only that the electron density lies between these two limits, the uncertainty in the predicted temperature increases with temperature, from ± 0.2 keV at 3 keV to ± 0.8 keV at 6 keV. The ratio was calculated in steady state, which is justified because the ionization times for Ne- and Na-like ions vary from 190 to 60 psec and from

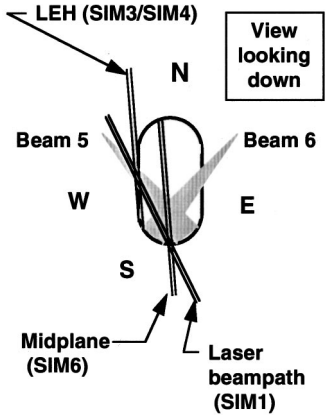

FIG. 2. Xe 4-2 spectra were measured from different views. Spectrographs were fielded in 6-in. manipulators (SIM's) on the Nova ten-beam target chamber and the effective source width in all cases was 80–140 μm. The illumination patterns of two laser beams are also shown.

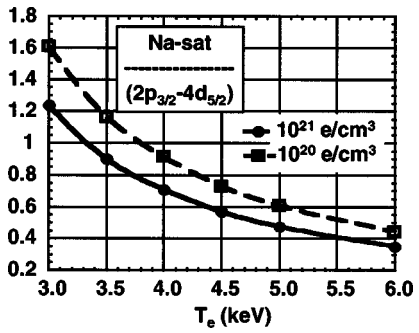

FIG. 3. The Xe 4-2 line ratio as a function of T_e for two different electron densities, 10^{20} and 10^{21} e/cm^3.

40 to 20 psec, respectively, for $3\ \mathrm{keV} \leqslant T_e \leqslant 6\ \mathrm{keV}$ and an electron density of 10^{21} e/cm^3.

RESULTS

To compare LASNEX predictions with the experiment, we have focused on the LEH line of sight. As noted above, we have concentrated our analysis on the 4-2 transitions, even though emission from 3-2 transitions were also detected. There are two reasons for this: first, the transitions corresponding to different ionization states (Ne, Na, Mg, etc.) are more clearly separated; and second, the lines should be more optically thin, reducing the importance of radiation transport. Radiation transport issues are also why we use the LEH line-of-sight data. We found that the LEH spectra vary as the laser power and gas fill change, while the spectra from other lines of sight do not. In particular, spectra acquired along the midplane line of site are remarkably constant. We attribute this to high line opacity, even for the 4-2 transitions. LASNEX predicts that the Xe plasma close to the hohlraum wall is much cooler than that directly heated by the laser beams.

An example of a Xe spectrum from the LEH line of sight is shown in Fig. 4. These data, recorded 1 nsec after the start of the laser pulse, correspond to a shot taken at low laser power with a 100% Xe fill. The spectrum is spatially resolved and indicates that the x-ray emission is contained within a radius of 0.5 mm, the region most strongly heated by the incident laser beams. A spectral lineout from the data shows the locations of the 4-2 lines used to estimate T_e, as well as the 3-2 lines. An example of how the 4-2 lines were

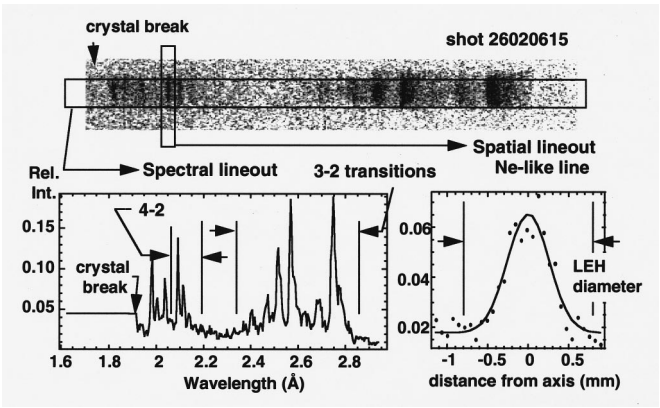

FIG. 4. A time- and space-resolved Xe spectrum obtained from a 100% Xe-filled hohlraum shot at low laser power (12.5 kJ).

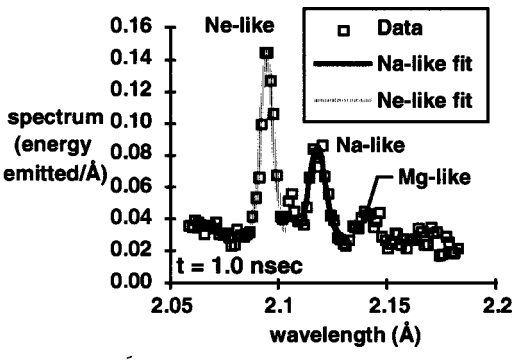

FIG. 5. Fitted Xe 4-2 spectrum obtained from a 100% Xe-filled hohlraum shot at low laser power (12.5 kJ). Analysis, using a 3.4×10^{20} e/cm^3 electron density (predicted by LASNEX), indicates $4.4\,\mathrm{keV}<T_e<5.3\,\mathrm{keV}$.

fit is given in Fig. 5. The uncertainties in the Ne- and Na-like line areas, which resulted in the stated T_e uncertainties, were estimated by comparing a Gaussian fit with a simple trapezoidal integration.

We used the ratio of the line areas to estimate the electron temperature, without additional compensations. Because the ionization rates ($\sim$30 psec for Na-like Xe, see above) are short compared to the laser heating pulse (1.4 nsec), the ionization balance, and therefore the line emission, is expected to track the plasma temperature. The signal-to-noise ratio is good because the line ratio is relatively close to unity, 0.4 to 1.4, in the expected temperature range. And the instrument response, which includes the photocathode sensitivity, crystal reflectivity, and pulsed gain uniformity of the GXI strip line, were assumed equal for the two lines because they are separated in energy by less than 0.06 keV and in space by less than 0.5 mm on the imager. Like this *L*-shell spectral approach, an isoelectronic *K*-shell (Ti/Cr or Ar/Cl) measurement [2–4] should have a good temporal response and signal-to-noise ratio, but the larger energy separation between the lines leads to uncertainties in the instrument response with respect to the photocathode efficiency, crystal reflectivity, and pulsed strip-line gain. On the other hand, a satellite to resonant line ratio measurement [5], for which the lines are physically close together on the imager, would have a relatively flat instrument response and, again, good temporal response. But the expected line ratios will be large, in the range of 10 to 40 or 100, which approaches the full linear dynamic range of a gated MCP device and limits the signal-to-noise ratio. The *L*-shell measurement has a fast temporal response, good signal-to-noise ratio, and a flat instrument response, but the line ratios are much more difficult to calculate because of the large number of transitions that contribute to the Na-like satellite line. The *L*-shell approach should find broader application as the computational tools required to predict the spectra become more widely available.

We find that agreement between LASNEX and the measurements is quite good. Table I summarizes the measurements and predictions at about 1 nsec from the start of the laser pulse. T_e was estimated from the ratio of the Ne- and Na-like line areas, using the electron density predicted by LASNEX, which was between 10^{20} and $10^{21}\,e/\mathrm{cm}^3$. Generally, T_e increases with increasing Xe fraction due to increased inverse Bremsstrahlung absorption. In all cases the values agree within the stated uncertainties. Because the sensitivity of the line ratio to T_e decreases with increasing T_e, the experimental uncertainties are larger at higher temperatures. The stated LASNEX uncertainty of 0.5 keV is an estimate based on limitations in the code's models for laser light absorption and heat conduction. This value may be high, since an uncertainty of 0.2 keV is all that is needed to obtain agreement with experiment.

The electron temperature increases with the *Z* of the gas fill, even though x-ray emission from the plasma increases as well. This is because inverse bremsstrahlung absorption [13] increases strongly with *Z*. An expression for the absorption coefficient is given below:

$$\kappa_{ib}=\frac{8n_e^2r_e^3\lambda_L^2}{3\sqrt{2\pi(1-n_e/n_c)}}\,\frac{Z\ln\Lambda}{T_e^{1.5}},$$

$$\Lambda\equiv\frac{cT_e}{\omega_p p_{\min}},$$

$$p_{\min}\equiv\max\left[\frac{Zr_e}{T_e},\frac{\lambda_e}{T_e^{0.5}}\right],$$

where n_e is the electron density (taken to be $0.1n_c$), r_e is the classical electron radius ($2.82\times10^{-13}\,\mathrm{cm}$), λ_L is the laser wavelength (0.351 μm), *Z* is the average charge state of the ions, n_c is the critical electron density corresponding to λ_L ($10^{22}\,\mathrm{cm}^{-3}$), T_e is the electron temperature in units of the electron rest mass (511 keV), *c* is the speed of light in vacuum, ω_p is the electron plasma frequency corresponding

TABLE I. T_e in laser entrance hole depends on fill gas and laser energy. Measurements are in good agreement with LASNEX predictions.

Gas fill	Laser energy (kJ)	T_e (keV) data (0.9–1.25 nsec)	T_e (keV) LASNEX (0.9 nsec)
100% Xe	30		5.9
67% Xe/33%D_2	30	5.5 ± 0.7	5.4
100% Xe	12.5	4.9 ± 0.4	4.3
70% Xe/30% C_5H_{12}	12.5	3.9 ± 0.3	4.0
50% Xe/50% C_5H_{12}	12.5	3.7 ± 0.1	3.6 ± 0.5

TABLE II. The much higher inverse bremsstahlung absorption in Xe will result in a higher T_e, in spite of increased extreme ultraviolet emission.

			T_e (keV)			
Fill	Z		0.5	1.5	3	6
Neopentane	2.5	Absorption length (mm)	0.82	3.62	9.35	24.31
Xe	44		0.07	0.27	0.64	1.56
		Ratio (neopentane/Xe)	11.02	13.41	14.58	15.56
Neopentane	2.5	Transmission to 2 mm	8.79%	57.58%	80.74%	92.10%
Xe	44	(Hohlraum wall location)	0.00%	0.06%	4.42%	27.80%

to n_e (1.69×10^{15} rad/sec), and λ_e is the Compton electron wavelength (3.86×10^{-11} cm). A number of values for the inverse bremsstrahlung absorption length ($\kappa_{\rm ib}{}^{-1}$) are given in Table II for neopentane (C_5H_{12}) and pure Xe fills, assuming that the neopentane is fully stripped and the Xe is in the neonlike ionization state. Shown as well are the ratio of the neopentane to Xe absorption length and the percentage transmission of the laser beam through 2 mm of plasma (about the distance from the LEH to the hohlraum wall along the laser beam path). Note that the volumetric heating rate of the plasma, given by the product of the laser intensity and the inverse bremstrahlung absorption coefficient, $I_L\kappa_{\rm ib}$, is 10 to 15 times higher for Xe at the LEH, where the laser first encounters the plasma. For this reason, even if greater than 75% of the incident laser energy is radiated away as UV and x-ray photons, there is sufficient absorbed energy to sustain an electron temperature that is 2–3 times higher in Xe, as compared to neopentane. Also, once the neopentane reaches 3 keV, over 80% of the incident laser energy is predicted to reach the hohlraum wall, while in the case of Xe this number is only 4%. Due to its higher Z, the Xe fill plasma can efficiently absorb the laser energy at higher electron temperatures, which increases the peak temperatures that can ultimately be reached.

CONCLUSIONS

In summary, we have estimated T_e in the LEH region of Xe-filled hohlraums from Xe 4-2 x-ray spectra, and have found the measurements to be in good agreement with LASNEX predictions, with $3.5\,{\rm keV}<T_e<6\,{\rm keV}$ for $10^{20}\,e/{\rm cm}^3<n_e<10^{21}\,e/{\rm cm}^3$. This agreement increases our confidence in LASNEX as an accurate modeling and predictive tool for these targets. These measurements are also important to understanding the growth and saturation of laser plasma instabilities for plasma conditions expected in NIF hohlraums [8]. New approaches are needed to obtain T_e measurements at the midplane of these targets, because plasma opacity and radiation transport cloud the issue. For T_e above 4 keV, K-shell emission from Kr and Br ($12\,{\rm keV}<E<13\,{\rm keV}$) may be useful for this measurement. A much more challenging goal is the measurement of the electron energy distribution function itself, rather than the moment corresponding to a temperature.

ACKNOWLEDGMENTS

We thank the Nova Operations Team, the Los Alamos technicians supporting Nova, the Target Fabrication Group at Los Alamos, K. Gifford (GA), and G. Stone (LLNL). This work was supported by the U.S. DOE.

[1] See, for example, B. J. MacGowan, B. B. Afeyan, C. A. Back, R. L. Berger, G. Bonnaud, M. Casanova, B. I. Cohen, D. E. Desenne, D. F. DuBois, A. G. Dulieu, K. G. Estabrook, J. C. Fernandez, S. H. Glenzer, D. E. Hinkel, T. B. Kaiser, D. H. Kalantar, R. L. Kauffman, R. K. Kirkwood, W. L. Kruer, A. B. Langdon, B. F. Lasinski, D. S. Montgomery, J. D. Moody, D. H. Munro, L. V. Powers, H. A. Rose, C. Rousseaux, R. E. Turner, B. H. Wilde, S. C. Wilks, and E. A. Williams, Phys. Plasmas **3**, 2029 (1996), and references therein.

[2] B. H. Failor, W. W. Hsing, R. G. Hockaday, T. D. Shepard, D. E. Klem, D. H. Kalantar, and B. J. MacGowan, Rev. Sci. Instrum. **66**, 767 (1995).

[3] C. A. Back, R. L. Berger, K. Estabrook, B. H. Failor, W. W. Hsing, E. J. Hsieh, R. Hockaday, D. H. Kalantar, R. L. Kauffman, C. J. Keane, D. E. Klem, B. J. MacGowan, D. S. Montgomery, J. D. Moody, L. V. Powers, T. D. Shepard, G. F. Stone, L. J. Suter, and R. E. Turner, J. Quant. Spectrosc. Radiat. Transf. **54**, 27 (1995).

[4] T. Shepard, C. A. Back, D. H. Kalantar, R. L. Kauffman, C. J. Keane, D. E. Klem, B. F. Lasinski, B. J. MacGowan, L. V. Powers, L. J. Suter, R. E. Turner, B. H. Failor, and W. W. Hsing, Rev. Sci. Instrum. **66**, 749 (1995); Phys. Rev. E **53**, 5291 (1996).

[5] S. H. Glenzer, C. A. Back, K. G. Estabrook, B. J. MacGowan, D. S. Montgomery, R. K. Kirkwood, J. D. Moody, D. H. Munro, and G. F. Stone, Phys. Rev. E **55**, 927 (1996), and references therein.

[6] J. Grun *et al.*, IEEE International Conference on Plasma Science Cat. No. 97CH36085, 1997, p. 124; C. A. Back, J. Grun, C. D. Decker, J. L. Davis, O. L. Landen, L. J. Suter, and R. Wallace, Applications of X Rays Generated from Lasers and Other Bright Sources [Proc. SPIE **3157**, 130 (1997)].

[7] B. H. Wilde *et al.*, in *Laser Interaction and Related Plasma Phenomena*, 12th International Conference, Osaka, 1995, edited by S. Nakai and G. A. Mileypu, AIP Conf. Proc. No. 369 (AIP, Woodbury, NY, 1996), p. 255.

[8] J. C. Fernandez, J. A. Cobble, B. H. Failor, D. F. DuBois, David S. Montgomery, Harvey A. Rose, Hoanh X. Vu, Bern-

hard H. Wilde, Mark D. Wilke, and Robert E. Chrien, Phys. Rev. Lett. **77**, 2702 (1996).

[9] J. C. Fernandez, J. A. Cobble, B. H. Failor, W. W. Hsing, H. A. Rose, B. H. Wilde, K. S. Bradley, P. L. Gobby, R. Kirkwood, H. N. Kornblum, D. S. Montgomery, and M. D. Wilke, Phys. Rev. E **53**, 2747 (1996).

[10] C. J. Keane, B. A. Hammel, A. J. Osterheld, and D. R. Kania, Phys. Rev. Lett. **72**, 3029 (1994).

[11] P. Beiersdorfer (private communication); P. Beiersdorfer, S. von Goeler, M. Bitter, E. Hinnov, R. Bell, S. Bernabei, J. Felt, K. W. Hill, R. Hulse, J. Stevens, S. Suckewer, J. Timberlake, A. Wouters, M. H. Chen, J. H. Scofield, D. D. Dietrich, M. Gerassimenko, E. Silver, R. S. Walling, and P. L. Hagelstein, Phys. Rev. A **37**, 4153 (1988).

[12] A. L. Osterheld *et al.*, Phys. Scr. **54**, 240 (1996).

[13] T. W. Johnston and J. Dawson, Phys. Fluids **16**, 722 (1973).